Helmholtz-Zentrum Geesthacht
Zentrum für Material- und Küstenforschung

Final Draft
of the original manuscript:

Dobron, P.; Balik, J.; Chmelik, F.; Illkova, K.; Bohlen, J.; Letzig, D.; Lukac, P.:
A study of mechanical anisotropy of Mg–Zn–Rare earth alloy sheet
In: Journal of Alloys and Compounds (2013) Elsevier

DOI: 10.1016/j.jallcom.2013.11.142

A study of mechanical anisotropy of Mg-Zn-Rare earth alloy sheet

Patrik Dobroň[a*], Jaroslav Balík[a], František Chmelík[a], Kseniya Illková[a], Jan Bohlen[b], Dietmar Letzig[b], Pavel Lukáč[a]

[a]*Charles University in Prague, Faculty of Mathematics and Physics, Department of Physics of Materials, Ke Karlovu 5, 12116, Prague 2, Czech Republic*
[b]*Helmholtz-Zentrum-Geesthacht, Zentrum für Material- und Küstenforschung GmbH, Max-Planck-Straße 1, D21502 Geesthacht, Germany*

ABSTRACT Rolled Mg-Zn-Rare earth sheet after annealing was deformed at room temperature with the tensile axis oriented in both the rolling and transversal direction. The deformation behaviour of the sheet has been investigated by acoustic emission (AE) and electron backscattered diffraction measurements, where the AE signal analysis correlates the microstructure and the stress-strain curves to the active deformation mechanisms. X-ray diffraction was applied to receive orientation images in order to characterize the deformation texture before and after the test.

Keywords: Metals and alloys; Mechanical properties, Scanning electron microscopy, SEM; X-ray diffraction;

*corresponding author: Tel.: +420 22191 1612 Fax: +420 22191 1490

E-mail:dobronp@karlov.mff.cuni.cz

1. Introduction

The recent developments in industrial applications of magnesium alloys are currently focused on the utilization of magnesium sheets. Mechanical properties (especially strength, ductility and formability) of wrought magnesium alloys which have hexagonal close packed (hcp) lattice are significantly influenced by strong textures [1]. The texture development and the deformation behaviour of magnesium alloys depend on the activation of both dislocation slip and twinning.

It is generally accepted that the tensile in-plane deformation in Mg alloy sheets is initially realized by dislocation glide in basal planes which later must be accomplished by a contribution of dislocation glide in non-basal planes and/or twinning. However, the operation of the individual non-basal slip systems and twinning with progressing plastic deformation is still being discussed by many authors. Some authors consider prismatic slip systems as more dominant [2, 3]. Hama and Takuda [2] who investigated the stress-strain curves obtained in cyclic loading-unloading tests of AZ31B magnesium alloy, have shown that basal and prismatic slip systems and tensile twinning were activated during loading while prismatic slip systems were hardly activated during inelastic unloading. They have also claimed that the activity of basal slip systems depends on the inhomogeneity of the samples. On the other hand, several investigators claim that homogeneous deformation is possible only when the second-order pyramidal slip systems are active, i.e. glide of (**c+a**) dislocations is necessary [4-7]. The activity of (**c+a)** dislocations in magnesium was found experimentally [8-10]. Using polycrystal plasticity modelling, Agnew and Duygulu [6] have shown that decreasing anisotropy of AZ31 with

increasing temperature may be explained by an increasing activity of the second-order pyramidal slip systems (increased (**c+a**) dislocation activity) and the primary (tensile) twinning mode [11].

Rolled sheets of the Mg-based alloys exhibit a typical basal texture with orientation of basal planes almost parallel to the sheet plane [12-14]. Such a texture favours deformation twinning if a compressive stress is applied along the rolling direction (RD) [15]. In the case of the tensile in-plane test, deformation can be realized practically without (near-zero) tensile twinning [6, 16]. Bohlen et al. [17] have recently reported the texture development in six Mg-Zn alloys with dilute additions of Y, Nd, Ce and Mn. It should be mentioned that the angular distribution of the basal poles in ZE10 is significantly broader to the transversal direction (TD); it is not affected in RD. On the other hand, the prismatic plane poles are mostly oriented parallel to RD. Therefore the strong basal texture is responsible for tension – compression asymmetry and anisotropy.

For the study of dynamic processes involved in plastic deformation of Mg alloy sheets, the acoustic emission (AE) technique can be efficiently used. It is based on sensitive detection of the transient elastic waves generated within the material during deformation due to sudden localized structure changes [18]. Detected AE signals can be parameterized according to their amplitude, number of counts, duration, energy or frequency. A direct correlation of AE parameters with the stress-strain curve yields information on the dynamic changes indicating e.g. activation of various deformation mechanisms during plastic deformation of Mg alloys [17, 19-21].

The aim of the present work is to examine deformation mechanisms occurring during tensile testing (along both RD and TD) of a ZE10 Mg alloy sheet by using *in situ* and *post mortem* methods, i.e. AE and electron backscattered diffraction (EBSD) respectively. The texture evolution was also measured. The stress dependence of the strain hardening rate and *in situ* AE were used in order to analyse deformation mechanisms during loading. Humps observed in the stress dependence of the strain hardening rates at the very beginning of strain are discussed. The measurement of the AE activity, represented by the AE count rate parameter, reveals dynamic changes in collective dislocation processes and possible twin nucleation during in-plane tensile tests under given conditions.

2. Experimental

Magnesium alloy ZE10 (Mg + 1.3 wt.% Zn+ 0.2 wt.% Ce + 0.1 wt.% La) was received as a rolled sheet of a thickness of 1.6 mm in the O temper condition. Pieces of the material were annealed for 1-16 hours at 300 °C to obtain a stress released condition (practically free of twins). Microhardness measurements were used to determine the lowest preliminary hardening state, in which the hardness value reaches a minimum. An annealing time of 6 hours was established.

Global texture information about the annealed and deformed sheets was obtained using X-ray diffraction. A Panalytical X-ray diffractometer setup using CuK_{α} radiation was employed to measure pole figures on polished samples in reflection geometry to a sample tilt of 70°. The texture analysis was conducted on the annealed sheet as well as on specimens after tensile testing to fracture.

Tensile specimens with a gauge length of 50 mm were machined from rolled sheet in the stress released conditions. Specimens were deformed along both RD and TD in a universal testing machine at room temperature (RT) and at a constant applied rate of 10^{-3} s^{-1}.

A computer-controlled DAKEL-IPL AE system based on continuous storage of AE signals with 2 MHz sampling frequency was used to monitor the AE activity. A miniaturized MIDI-410-2 piezoelectric transducer (diameter 6 mm) was attached to the specimen surface with the help of silicon grease and a spring. A preamplifier with a gain of 35 dB was used. After the measurement, threshold-level detection of recorded AE signals was done to achieve a comprehensive set of AE parameters. The threshold voltage for the AE count rate $\Delta N_C/\Delta t$ (number of counts per second [22]) was 15 % of the maximum voltage (2.4 V).

Four samples were stressed to specific points on the deformation curve (where significant changes in the AE activity were observed) and then EBSD was used to analyze the sample microstructure in a field emission gun scanning electron microscope (Zeiss Ultra 55, EDAX/TSL EBSD system and Hikari detector) on electropolished longitudinal sections. Special attention was given to the formation of twins, their type and distribution.

3. Results

The inverse pole figure (IPF) map and grain size distribution after rolling process are presented in Fig. 1. Sheet exhibits a typical microstructure consisting from elongated grains into RD with average grain size of 16 μm. The initial textures and the textures after tensile deformation in RD and TD of the rolled ZE10 magnesium alloy sheet are shown

as pole figures in Fig. 2. The textures are represented by the distribution of basal (0002) and prismatic $(10\bar{1}0)$ poles. In the initial state, the pole figure (0002) of ZE10 sheet displays texture with the orientation of basal planes tilted away from the plane of the sheet (normal direction (ND)). The intensity of basal planes in the (0002) pole figure significantly varies with respect to RD and TD – the basal poles are broader tilt and splitting towards TD rather than to RD. The characteristic angular spread of basal planes with a double peak towards TD is observed. The $(10\bar{1}0)$ pole figure has the highest intensity in RD. Such a texture is different from a texture observed in conventional magnesium alloy sheets, such as AZ31. It is interesting to note that Mackenzie and Pekguleryuz [8] have observed similar characteristics of the ZE10 texture. They investigated the texture evolution in rolled and annealed Mg-1Zn alloys with the addition of cerium. Weak non-basal textures were observed in Mg-1Zn-0.3Ce alloy sheets.

Tensile tests along RD cause angular spread of basal fibres towards TD direction, but the highest intensity of the $(10\bar{1}0)$ pole figure in RD still persists. Tension along TD causes angular spread of basal fibres towards RD i.e. perpendicular to the tensile axis, similarly as in the RD loading, and the $(10\bar{1}0)$ pole figure shows 6-fold symmetry with peak intensity into TD.

Figure 3 shows the true stress–true strain and work hardening-true stress curves with corresponding AE response for tension along RD and TD. The mechanical behaviour is significantly influenced by texture. In-plane anisotropy of the yield strength (YS) between RD and TD sample is clearly seen; a higher value of YS for RD sample than TD one is observed. Likewise, differences in the AE response are observed. It is important to

note that the reverse is observed during straining of rolled AZ31 magnesium alloys. The strength of TD AZ31 samples is higher than that of RD ones as reported e.g. by Agnew and Duygulu [6]. From the stress-strain curves (Fig. 3) it is obvious that the tensile direction has a strong influence on the tensile deformation behaviour of ZE10 sheets. This deformation behaviour can be better seen from the Kocks-Mecking plots [23], i.e. the plots of the strain hardening rate, θ, against the flow stress, σ. A qualitatively difference in the form of the initial parts of the Kocks-Mecking plots, for both RD- and TD-regimes, is shown in Fig. 3 (bottom). The strain hardening did not decrease monotonically with stress as observed in fcc metals. It can be seen that in the early straining stages, the strain hardening rate first decreases rapidly, then increases with increasing stress and after an increase again decreases with stress. A hump (hereafter referred to as lift), occurring in the stress dependence of the strain hardening rate, is less pronounced and narrower for RD-regime than that for TD sample.

It can be seen that the AE activity starts at a lower flow stress in RD than in TD samples. The AE count rate exhibits a peak at the beginning of plastic deformation which is much more pronounced for TD than for RD samples (10^5 for TD samples and 10^3 for RD ones). The AE count rate for the narrow lift observed in the samples deformed in RD direction goes rapidly to zero, while that for the broad one in TD samples persists almost constant.

The EBSD analysis was performed on four samples which were stressed to different states of deformation (marked as A, B, C and D position in Fig. 3) in order to study twinning activity (significant changes in the AE activity). Pole figures obtained from EBSD measurements are presented in Fig. 4. Gray points represent original texture after

rolling process and black points symbolize twinning activity. Twin fraction was calculated from IPF maps.

4. Discussion

The presented results indicate different micromechanisms responsible for the strain hardening behaviour of ZE10 Mg alloy sheet deformed along both RD and TD. Texture analysis and AE measurements during straining are useful (and successful) tools indicating the microstructural evolution (dislocation evolution, twinning) and they may help to estimate deformation micromechanisms. Likewise, the strain hardening behaviour may be analysed using the stress dependence of the strain hardening rate. As mentioned above, the form of the hardening lift is different for samples deformed in RD and TD. The hardening lift in the TD sample extends over a wide flow stress range (Fig. 3, bottom). The concurrent AE measurements show that collective dislocation processes start at a lower flow stress in RD than in TD, which points out that the primary (basal) slip mechanism can be easier activated in RD. The characteristic AE peak at the onset of plastic deformation for samples deformed in both RD and TD is usually explained by a massive dislocation multiplication when basal and non-basal slip systems are activated. The lower and broader AE peak (near the yield point) observed for samples deformed in RD can be assumed as a consequence of the AE activity before the yield point. The subsequent strong decrease in the AE count rate for the narrow lift observed in the samples deformed in RD can be explained by increasing number of sessile dislocations, which reduce the free path of moving dislocations. In the case of the samples deformed in TD, the AE count rate remains practically constant during the wide hump (lift), which

indicates the presence of twinning. Furthermore, S - shape of the deformation curve is a typical sign of twinning activity.

The EBSD analysis was performed on four samples which were stressed to different states of deformation (marked as A, B, C and D position in Fig. 3) in order to support the explanation of the AE results. The significant twinning during tension in TD is presented in Fig. 3b (black points). The twin fraction was estimated to be 0.071 and 0.10 at the lower (position C) and higher (position D) deformations, respectively. Twin nucleation is an excellent source of detectable AE activity [24]. It has been reported in [24, 25] that the twin growth does not produce AE contrary to the twin nucleation. Therefore, the plateau in the count rate following the peak in TD is consistent with twin nucleation. For RD - testing, much smaller twin fractions, 0.009 and 0.036 (Fig. 4a, A and B position), respectively, were estimated. Considering the presence of some twins in the initial state and a substantially lower level of AE, thickening of preexisting twins rather than the nucleation of new ones may be supposed for samples deformed in RD by tension.

Likewise, Dobroň et al. [26] have proven with the help of EBSD measurements that an increase in the AE count rate despite of a strong strain hardening in extruded AZ31 is caused by the twinning activity.

It should be mentioned that the lift in the stress dependence of the strain hardening rate observed in ZE10 specimens deformed in RD has a similar form as that observed in θ vs. σ plots for the annealed rolled AZ31 magnesium alloy sheets deformed in both RD and TD [27]. Balík et al. [30] have concluded that such deformation behaviour can be connected with the activity of double prismatic slip. We assume that the lift in the stress

dependence of the strain hardening rate for ZE10 deformed in RD is related to the transition from primary (basal) to secondary (non-basal) slip mechanisms. We suppose likewise that the non-basal slip systems responsible for the lift in RD specimens are the prismatic planes with glide (cross-slip) of dislocations with the <**a**> type Burgers vectors [28, 29]. This is in agreement with observations of the prismatic slip of <**a**> dislocations in *in-situ* TEM experiments presented by Couret and Caillard [30].

On the other hand, the wider lift in the stress dependence of the strain hardening rate obtained for samples deformed in TD is a result of twinning.

5. Conclusions

The strain hardening rate vs. the flow stress plots for sheet deformed in RD and TD was used to analyse the hardening behaviour. The break in the monotonous stress dependence of the strain hardening rate – an increase in the strain hardening rate is observed at very low strain. Whereas the fairly narrow lift during RD loading seems to correspond to the transition from the initial basal slip to a secondary double prismatic slip, the broader lift in TD loading indicates the nucleation of the tensile twins. The AE and EBSD measurements that differ obviously for RD and TD loading support these suggestions as well. The results presented in this work show an effective way on how the stress dependence of the strain hardening rate connected with the AE and EBSD analyses can be of great importance for revealing deformation mechanisms.

Acknowledgement

This work received support from the Czech Science Foundation under grant 13 - 19812S and the work of P.D. is a part of activities of the Charles University Research Center

"Physics of Condensed Matter and Functional Materials". F.C. is grateful to the Alexander von Humboldt Stiftung for financial support during his stay in Germany.

References

[1] C.J. Bettles, M.A. Gibson, JOM - J. Min. Met. Mat. S. 57 (2005) 46.

[2] T. Hama, H. Takuda, Int. J. Plasticity 27 (2011) 1072.

[3] C.J. Boehlert, Z. Chen, I. Gutiérrez-Urrutia, J. Llorca, M.T. Pérez-Prado, Acta Mater. 60 (2012) 1889.

[4] F.F. Lavrentev, Mater. Sci. Eng. A 46 (1988) 191.

[5] P. Lukáč, Czech. J. Phys. B 35 (1985) 275.

[6] S.R. Agnew, O. Duygulu, Int. J. Plasticity 21 (2005) 1161.

[7] S. Sandlöbes, S. Zaeffere, I. Schestakow, S. Yi, R. Gonzalez-Martinez, Acta Mater. 59 (2011) 429.

[8] T. Obara, H. Yoshinaga, S. Morozumi, Acta Metall. 21 (1973) 845.

[9] H. Yoshinaga, R. Horiuchi, Trans. JIM 5 (1964) 14.

[10] S. Ando, T. Mayasuki, K. Hiromoto, Mater. Sci. Forum 654-656 (2010) 699.

[11] D.W. Brown, S.R. Agnew, M.A.M. Bourke, T.M. Holden, S.C. Vogel, C.N. Tomé, Mater. Sci. Eng. A 399 1-2 (2005) 1.

[12] L.W.F. Mackenzie, M.O. Pekguleryuz, Scripta Mater. 59 (2008) 665.

[13] S.B. Yi, J. Bohlen, F. Heinemann, D. Letzig, Acta Mater. 58 (2010) 592.

[14] K. Hantzsche, J. Bohlen, J. Wendt, K.U. Kainer, S.B. Yi, D. Letzig, Scripta Mater. 63 (2010) 725.

[15] R.E. Reed-Hill, Am. Soc. Metals 285 (1973) 311.

[16] A. Jain, S.R. Agnew, Mater. Sci. Eng. A 462 (2007) 29.

[17] J. Bohlen, M.R. Nürnberg, J.W. Senn, D. Letzig, S.R. Agnew, Acta Mater. 55 (2007) 2101.

[18] C.R. Heiple, S.H. Carpenter, J. Acoustic Emission 6 (1987) 177.

[19] J. Bohlen, F. Chmelík, P. Dobroň, F. Kaiser, D. Letzig, P. Lukáč, K.U. Kainer, J. Alloy Compd. 378 (2004) 207.

[20] P. Dobroň, J. Bohlen, F. Chmelík, P. Lukáč, D. Letzig, K.U. Kainer, Kovove Mater. 45 (2007) 129.

[21] A. Vinogradov, D. Orlov, A. Danyuk, Y. Estrin, Acta Mater. 61 (2013) 2044.

[22] Standard Practice for Acoustic Emission Examination of Fiberglass Reinforced Plastic Resin, ASTM E 1067-85. Tank/Vessels, May 31, 1985.

[23] U.F. Kocks, H. Mecking, Progr. Mater Sci. 48 (2003) 171.

[24] C.R. Heiple, S.H. Carpenter, J. Acoustic Emission 6 (1987) 215.

[25] J.P. Toronchuk, Mater. Eval. (1977) 51.

[26] P. Dobroň, F. Chmelík, S.B. Yi, K. Parfenenko, D. Letzig, J. Bohlen, Scripta Mater. 65 (2011) 424.

[27] J. Balík, P. Lukáč, Z. Drozd, R. Kužel, Int. J. Mat. Res. 100 (2009) 322.

[28] J. Balík, P. Lukáč, R. Kužel, Acta Phys. Polonica A (2012) 435.

[29] M.R. Barnett, Z. Keshavarz, X. Ma, Metall. Mater. Trans. A 37 (2006) 2283.

[30] A. Couret, D. Caillard, Acta Metall. 33 (1985) 1447.

Fig. 2. Crystallographic texture of rolled ZE10 before and after the tensile test along the RD and TD.

Fig. 3. Stress-strain and strain hardening rate-stress curves correlated with the AE count rate for a) rolling direction and b) transversal direction.

Fig. 4. Local EBSD orientation data (a) RD positions A, B (see Fig. 3a)

(b) TD positions C, D (see Fig. 3b)

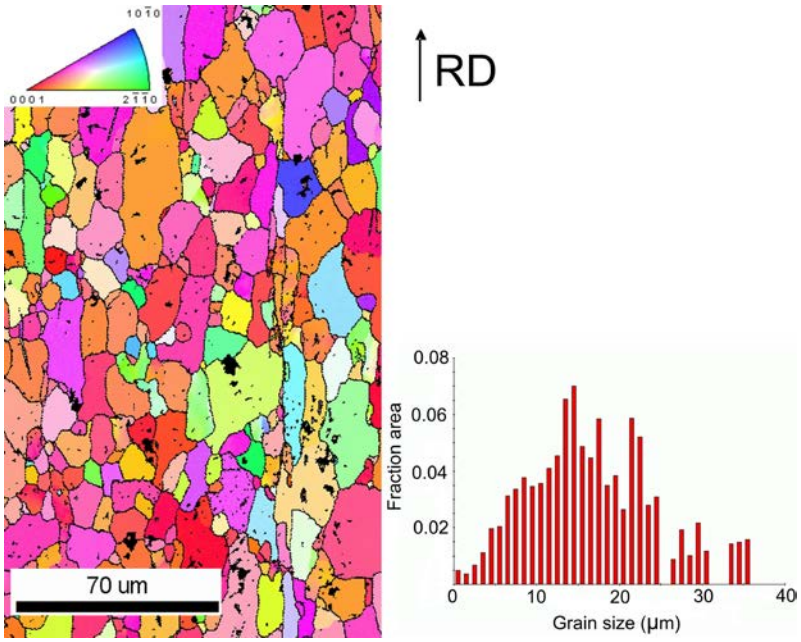
RD
70 um
Fraction area
0.08
0.06
0.04
0.02
0
10
20
30
40
Grain size (μm)

Fig. 1

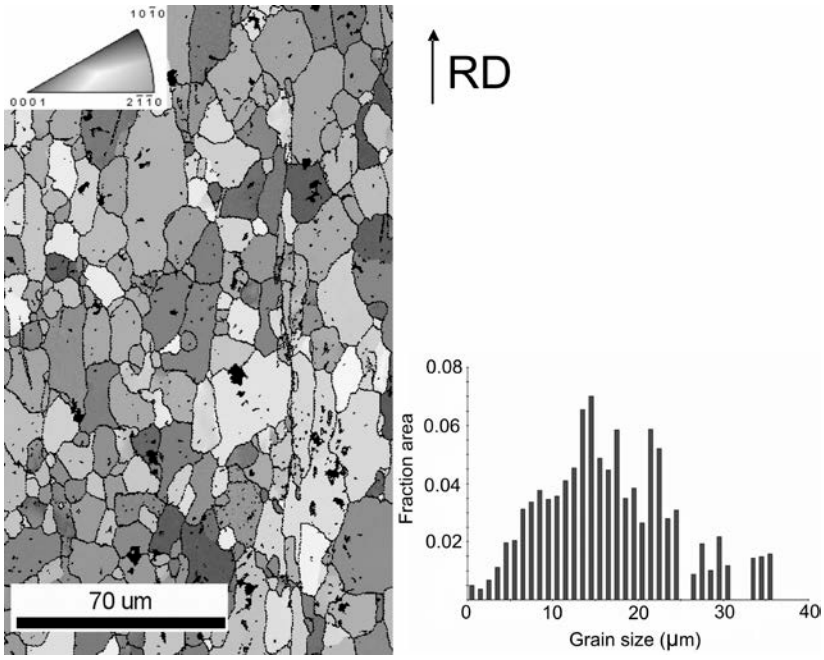
RD
70 um
Fraction area
0.08
0.06
0.04
0.02
0
10
20
30
40
Grain size (μm)

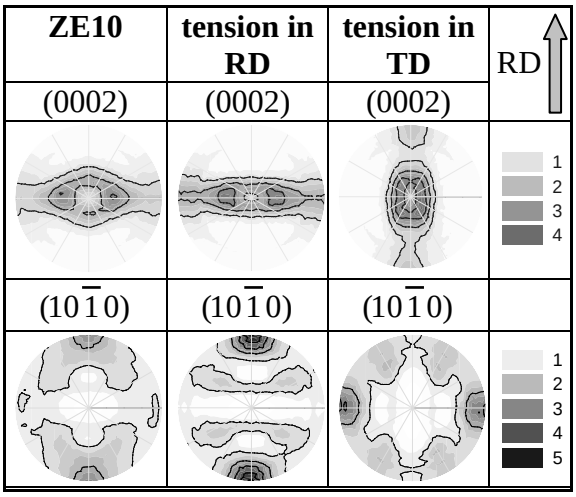
ZE10
tension in RD
tension in TD
RD
(0002)
(0002)
(0002)
1
2
3
4
(10$\bar{1}$0)
(10$\bar{1}$0)
(10$\bar{1}$0)
1
2
3
4
5

Fig. 2

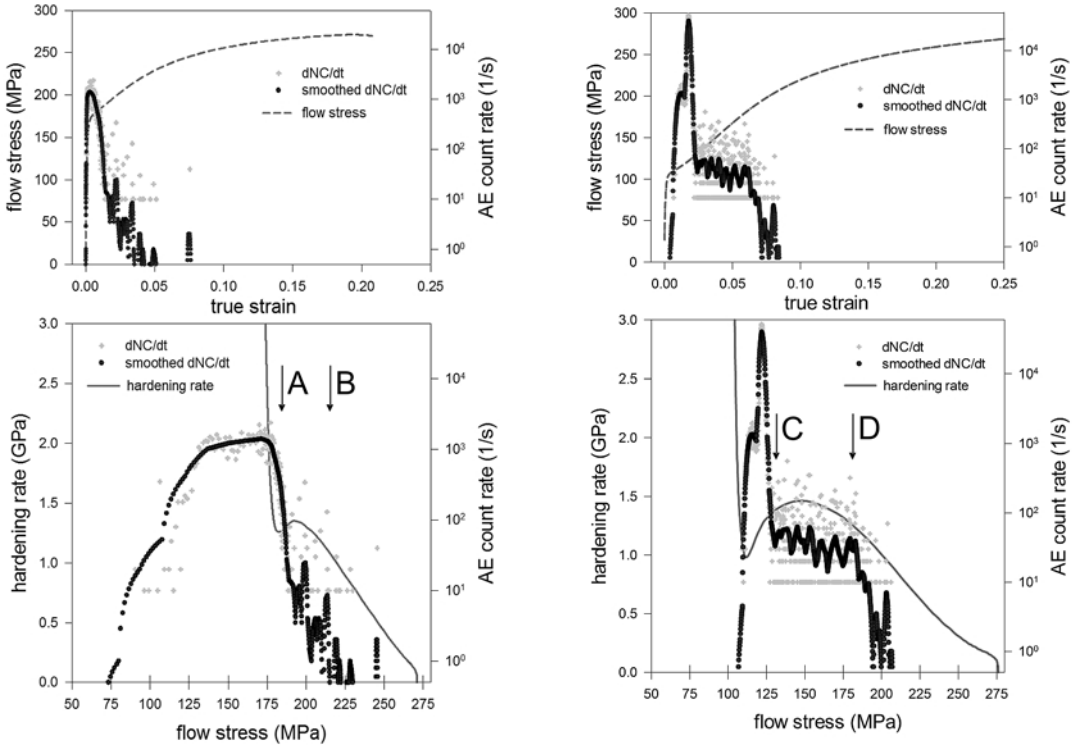
flow stress (MPa)
AE count rate (1/s)
true strain
dNC/dt
smoothed dNC/dt
flow stress
hardening rate (GPa)
hardening rate
A
B
C
D
flow stress (MPa)

Fig. 3

a) b)

a) A B

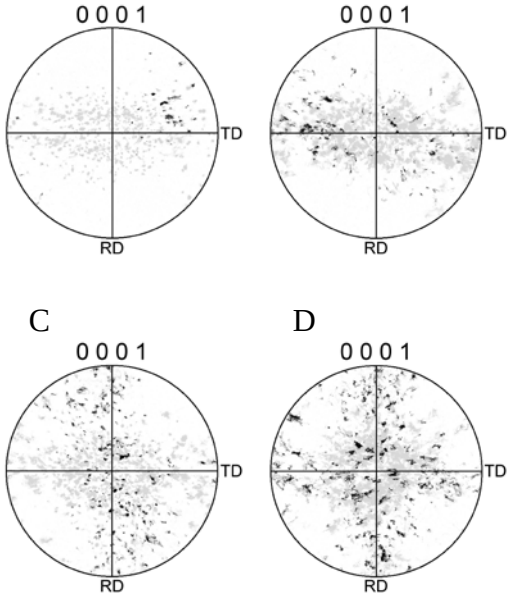

b)

Fig. 4